Rogue waves of the Sasa-Satsuma equation in a chaotic wave field

J. M. Soto-Crespo,[1] N. Devine,[2] N. P. Hoffmann,[3,4] and N. Akhmediev[2]
[1]*Instituto de Óptica, C.S.I.C., Serrano 121, 28006 Madrid, Spain*
[2]*Optical Sciences Group, Research School of Physics and Engineering, The Australian National University, Canberra ACT 0200, Australia*
[3]*Dynamics Group, Hamburg University of Technology, 21073 Hamburg, Germany*
[4]*Department of Mechanical Engineering, Imperial College, London SW7 2AZ, United Kingdom*
(Received 24 March 2014; published 2 September 2014)

We study the properties of the chaotic wave fields generated in the frame of the Sasa-Satsuma equation (SSE). Modulation instability results in a chaotic pattern of small-scale filaments with a free parameter—the propagation constant k. The average velocity of the filaments is approximately given by the group velocity calculated from the dispersion relation for the plane-wave solution. Remarkably, our results reveal the reason for the skewed profile of the exact SSE rogue-wave solutions, which was one of their distinctive unexplained features. We have also calculated the probability density functions for various values of the propagation constant k, showing that probability of appearance of rogue waves depends on k.

DOI: 10.1103/PhysRevE.90.032902 PACS number(s): 05.45.Yv, 42.65.−k, 47.20.Ky

I. INTRODUCTION

Studies of rogue waves in recent years are becoming extensive [1–4]. The subject has a great relevance for seafarers as it is important for them to avoid rogue waves in the open ocean [5–7]. It is also an interesting object in science as researchers want to understand the physics behind the phenomenon [8–10]. The field also provides sufficient material for mathematicians as rogue waves can be studied using rigorous analytical tools [11–14]. Moreover, the concept of rogue waves is presently emerging in many other branches of science [15–19] and even in finances [20].

The research naturally started with the simplest nonlinear mathematical model, which is the nonlinear Schrödinger equation (NLSE) [21]. This approach allowed us to find unexpected solutions, even for this well-known equation [22,23]. However, the NLSE has limitations related to the approximations used in its derivation [24,25]. Extending these techniques for finding solutions to more general models [26] must be the next step in the rogue-wave research.

The Sasa-Satsuma equation (SSE) is one of the known integrable extensions of the NLSE. It contains the most essential contributions often found in important physical applications, such as dynamics of deep water waves [27,28], pulse propagation in optical fibers [29,30], and generally in dispersive nonlinear media [31]. Namely, it contains the terms describing third-order dispersion, self-frequency shift, and self-steepening in fixed proportions that make it integrable. According to the original work of Sasa and Satsuma [32], the equation can be written in the form

$$i\psi_\tau + \frac{\psi_{xx}}{2} + |\psi|^2\psi = i\epsilon[\psi_{xxx} + 3(|\psi|^2)_x\psi + 6|\psi|^2\psi_x]. \tag{1}$$

Here, the arbitrary real parameter ϵ scales the integrable perturbations of the NLSE. When $\epsilon = 0$, Eq. (1) reduces to the standard NLSE, which has only the terms describing lowest order dispersion and self-phase modulation.

There is a number of publications dealing with the solutions of the SSE [33–39]. The form of Eq. (1) has been used in a series of works by Mihalache *et al.* [33–35]. The form of the SSE in the work by Wright III [36] is slightly different from the original version:

$$ip_t - p_{xx} - 2|p|^2p = i\delta[p_{xxx} - 3(|p|^2)_xp + 6(|p|^2p)_x]. \tag{2}$$

Equations (1) and (2) can be mutually converted one into the other using the following transformation:

$$\psi(x,t) = p^*(x,t), \quad \tau = 2t, \quad \delta = 2\epsilon. \tag{3}$$

This means that we can easily transform solutions of one equation into solutions of the other using Eq. (3). Also, changing the sign of ϵ or δ is equivalent to changing the direction in x. Keeping this symmetry property in mind, without loss of generality, we can restrict ourselves to consider only positive values of ϵ. Here, we will only present the results for Eq. (1).

II. PLANE-WAVE SOLUTION

Analytical solutions for rogue waves are always located on a plane-wave background. The latter serves as the source from which the emerging rogue wave acquires its energy. The Sasa-Satsuma Eq. (1) admits the family of plane-wave solutions given by

$$\psi_0(x,\tau) = -\frac{c}{2\epsilon}\exp\left[i\left(\frac{k}{2\epsilon}x - \frac{\omega}{8\epsilon^2}\tau\right)\right], \tag{4}$$

where the amplitude parameter c, the wavenumber k, and the frequency ω are coupled through the dispersion relation

$$\omega = k^3 + k^2 - 6c^2k - 2c^2. \tag{5}$$

The solution has two free independent parameters, c and k. It looks singular with respect to the equation parameter ϵ. However, this singularity is deceptive. Namely, when taking the NLSE limit, $\epsilon \to 0$, we can choose c and k to be linearly proportional to ϵ. Taking, in addition, $\omega \sim \epsilon^2$ eliminates the singularity.

Equation (1) is normalized in a way that the coefficients in the NLS part of the equation are set to $1/2$ in front of the diffraction term ψ_{xx}, and 1 in front of the nonlinear term

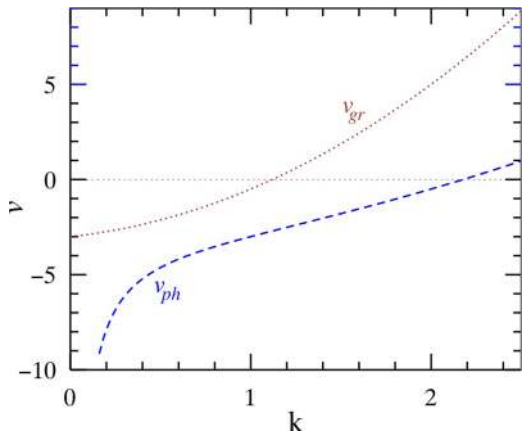

FIG. 1. (Color online) Phase (dashed blue lower curve) and group velocities (dotted brown upper curve) of the plane wave for $c = 2\epsilon = 1$. In the interval of k values [1.12,2.18], they have opposite signs.

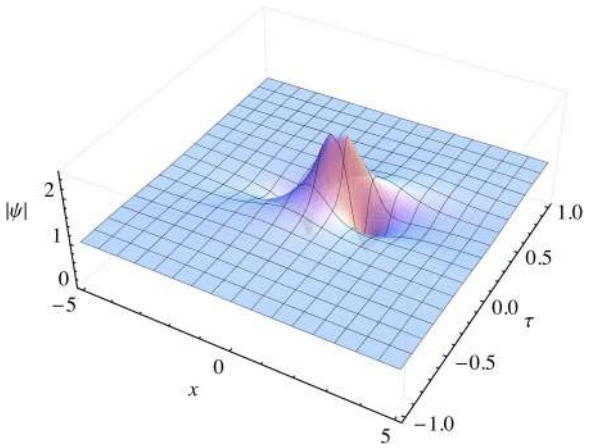

FIG. 2. (Color online) Rogue wave of the SSE at the threshold of transition to the one-peak case. Parameters $c = 1$, $\epsilon = 0.5$, and $k = 2$. The rogue wave is skewed to the right.

$|\psi|^2\psi$. This choice sets the mutual scaling of the variables. For consistency, we consider normalized solutions of Eq. (1). Thus, without restricting generality, we shall deal with plane waves with the amplitude set to one. This means that we can choose the parameter c to be equal to 2ϵ. This is the choice that we keep in all numerical simulations below. This, in turn, means that the only free parameter of the plane-wave solution is k.

One important conclusion from the expression for the plane wave is that the group velocity is different from the phase velocity. From Eq. (4), we can easily deduce that the phase velocity of the plane wave is given by

$$v_{\rm ph} = \frac{1}{4\epsilon}\frac{\omega}{k} = \frac{k^2 + k - 6c^2 - 2c^2/k}{4\epsilon}. \tag{6}$$

The k-dependence of the phase velocity, for $c = 2\epsilon = 1$, is shown in Fig. 1 by the dashed blue line. The phase velocity is negative in most of the region of interest and becomes largely negative at k values approaching zero.

On the other hand, the group velocity calculated from Eqs. (4) and (5) is

$$v_{\rm gr} = \frac{1}{4\epsilon}\frac{\partial\omega}{\partial k} = \frac{3k^2 + 2k - 6c^2}{4\epsilon}. \tag{7}$$

The k dependence of the group velocity is shown in Fig. 1 by the dotted brown curve. As we can see, the group velocity is negative at small k and becomes positive above $k \approx 1.12$. In the interval of k values [1.12,2.18], the two velocities have different signs. This feature is quite different from the NLSE case.

III. ROGUE-WAVE SOLUTIONS

The exact rogue-wave solution of the SSE has been presented for the first time in the work [40]. The solution is cumbersome and will not be reproduced here. Remarkably, it contains the same two free parameters (k,c) as the plane wave on which it resides. The third one is ϵ, which is the parameter of the equation.

Three examples of rogue-wave solutions are shown in Figs. 2, 3, and 4. These different types of solutions are typical of the three regions of k we are dealing with. The solution has a single peak when k is higher than $k = 2$ (see Fig. 2). It has two peaks when k is smaller than 2. An example when $k = 0.8$ is shown in Fig. 3. The solution is also skewed in the opposite direction. For even smaller k values the solution keeps a double-peak structure and becomes elongated keeping the same skew direction. The representative case $k = 0.25$ is shown in Fig. 4. In these three cases, we have kept parameters c and ϵ fixed in such a way that the background $c/(2\epsilon)$ remains constant $= 1$, namely we used $c = 1$ and $\epsilon = 0.5$.

The same rogue-wave solution as in Ref. [40] was later rederived by Shihua Chen in Ref. [41]. The expression given in Ref. [41] is simply translated along the τ and x axes in comparison to the original result [40]. The solution given in Fig. 4 is called in Ref. [41] "twisted pair," although in reality, the double-peak solution at small k is just becoming elongated as Fig. 4 shows.

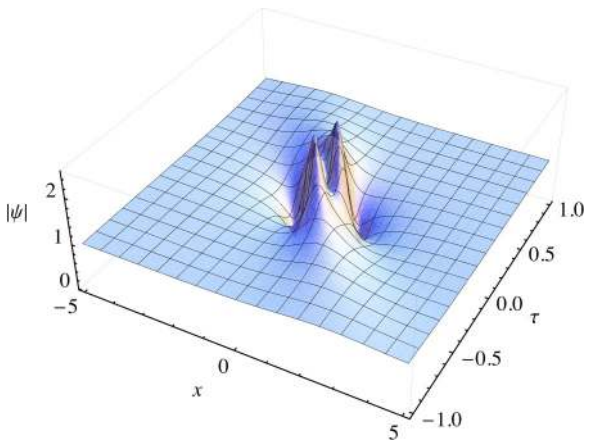

FIG. 3. (Color online) Rogue wave of the SSE with two peaks. Parameters $c = 1$, $\epsilon = 0.5$, and $k = 0.8$. The rogue wave is skewed to the left.

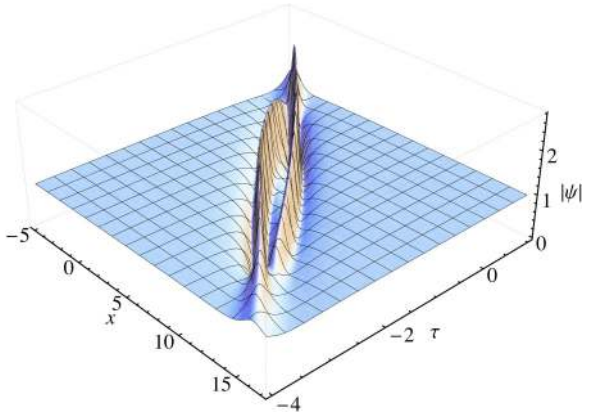

FIG. 4. (Color online) Rogue wave of the SSE with parameters $c = 1$, $\epsilon = 0.5$, and $k = 0.25$. Rogue waves become more and more elongated at lower values of k and get a stronger tilt to the left.

In addition to changing the profile of the rogue wave, the rogue-wave solution also changes its orientation in the (x,τ) plane with changing the parameter k. As we can see from the above figures, the solutions are skewed with respect to the τ axis. When $k = 2$, the solution is skewed to the right while in the other two cases, $k = 0.8$ and $k = 0.25$, the rogue wave is skewed to the left. This observation is in agreement with the change of sign of the group velocity at $k = 1.12$ in Fig. 1. This feature had been observed before [40] but was presented without any explanation. Interestingly, this tilt also appears in the orientation of the waves created in a chaotic wave field. This similarity serves as a basis for the explanation of this interesting feature of SSE rogue waves. Below, we will use the above-mentioned three values of k in order to demonstrate the difference this parameter makes when we are dealing with a chaotic wave field.

IV. CHAOTIC WAVE FIELDS

Processes described by a dynamical system such as the SSE can be highly complicated. However, they are still governed by a partial differential equation and can be predicted once the initial condition is given. Thus, in contrast to true stochastic processes, which are completely unpredictable, the processes in our system are "chaotic." Therefore, we use this term throughout the paper.

In systems with three-dimensional phase space, chaotic dynamics is related to exponentially diverging trajectories. Our system is infinite-dimensional. It is significantly more complicated than those usually considered in nonlinear dynamics. Nevertheless, different frequency components of the initial condition in our system exponentially diverge too. This can be seen from the fact that the growth rates of modulation instability (MI) for various spectral components differ. Thus, for initial conditions containing many frequencies, the total dynamics quickly enters a chaotic regime of evolution. Being described by a differential equation, this chaotic regime can be called deterministic. On the other hand, various realizations that start with different initial conditions may feature elements of true stochasticity just because of the stochasticity of the initial conditions. This additional complication makes a difference between systems with infinite-dimensional phase space and simpler ones usually considered in existing textbooks on chaotic dynamics.

We have numerically solved the SSE, taking as initial condition the plane-wave solution Eq. (4) perturbed with white noise of small amplitude. Namely, as initial condition we use the function

$$\psi(x,\tau = 0) = \psi_0(x,0) + \mu f(x),$$

where $\psi_0(x,0)$ is given by Eq. (4) with $\tau = 0$, μ is a small real parameter, and $f(x)$ is a complex function, whose real and imaginary parts are uncorrelated random functions uniformly distributed in the interval $[-1,1]$ generated by a standard random computer function. This random function contains all spectral components with roughly equal amplitudes.

For the numerical simulations, we used a split-step Fourier technique, solving the linear part in Fourier space and the nonlinear part with a fourth-order Runge-Kutta method. The mesh size in x axis varied from 0.005 to 0.01, depending on the total size of the x interval, while the step size in τ axis was fixed and equal to 0.00001. This choice provided stability of the scheme for all numerical runs.

Modulation instability seeded by the above noise creates a chaotic wave field that starts from this initial plane wave. An example of a wave field generated this way is shown in Fig. 5 for $k = 2$. The figure shows in a color code the field amplitude versus x and τ. The initial part ($0 < \tau < 0.5$) is not shown in the figure as the deviations from the plane-wave solution are small and the field amplitude is very close to 1 for all x. As expected, the spectral component of the noise with the highest

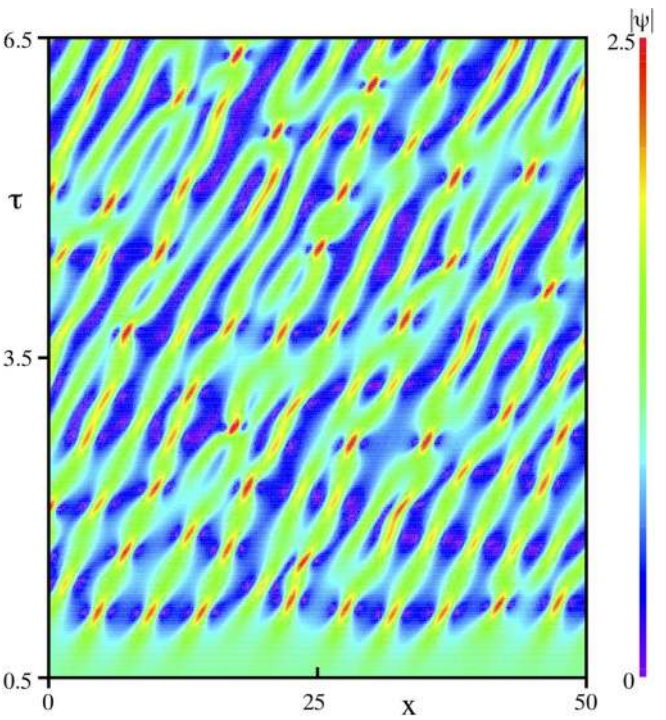

FIG. 5. (Color online) A typical example of a chaotic wave field created by the SSE that starts with modulation instability. Parameter $k = 2$. Most of the waves have a one-peak structure. Filaments are propagating to the right with average group velocity $v_{gr} \approx 5$.

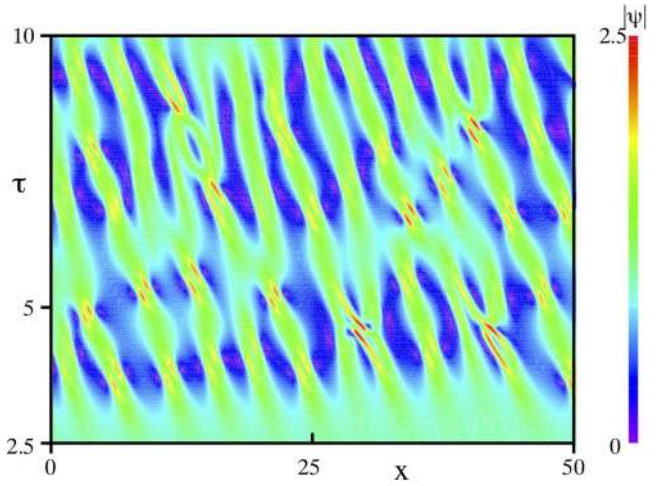

FIG. 6. (Color online) Chaotic wave field created by the SSE that starts with modulation instability. The wave number $k = 0.8$. Most of the maxima are grouped in pairs. Filaments propagate to the left due to the negative group velocity.

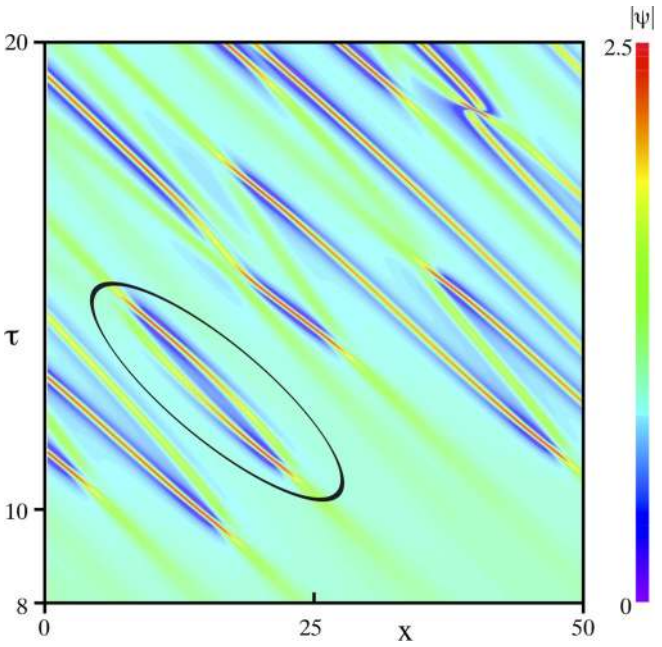

FIG. 7. (Color online) Chaotic wave field created by the SSE that starts with modulation instability. Parameter $k = 0.25$. Some of the big waves have an elongated two-peak structure similar to the rogue wave shown in Fig. 4. One example is encircled by the black ellipse. Filaments are propagating to the left at a larger angle than in the case $k = 0.8$.

growth rate dominates and splits the plane wave into filaments. The presence of other frequencies ensures that the filaments evolve chaotically. Figure 5 shows one realization of many thousands that we conducted in our work. For the statistical plots presented below, we used 5 000 realizations each running from $\tau = 0$ to 40.

In contrast to the NLSE case, the filaments here have a preferential direction of propagation with nonzero velocity. This happens because the group velocity of the waves is different from the phase velocity. The velocity of these filaments can be estimated from the expression for the group velocity [Eq. (7)]. When $k = 2$, the group velocity is positive, $v_{gr} = 5$. This agrees well with the average velocity of the filaments observed in Fig. 5.

Occasionally, the filaments collide or become narrower creating maxima at certain points of the wave field. These maxima can be seen in this figure in the form of red spots. These red spots essentially have a single maximum and are slightly elongated in the same way as the rogue wave seen in Fig. 2. The orientation of the peak elongations is the same as in Fig. 2. Moreover, the direction of these elongations is roughly the same as the orientation of the filaments. This means that the direction is given by the group velocity [Eq. (7)]. Thus, even the orientation of the rogue waves on the (x,τ) plane roughly can be estimated using Eq. (7).

This conjecture is further confirmed by the plot shown in Fig. 6. This chaotic wave field is generated for the case $k = 0.8$. The group velocity changes sign at approximately $k \approx 1.12$. It is negative $v_{gr} = -1.24$ for $k = 0.8$. The filaments in Fig. 6 propagate to the left in agreement with this prediction. The peaks of the chaotic wave field are also elongated and have roughly the same orientation as the filaments. Remarkably, this also agrees with the orientation of the rogue wave shown in Fig. 3. Moreover, the big waves in Fig. 6 have two maxima, just like the rogue wave in Fig. 3. These double maxima are clearly visible in red color in Fig. 6.

Additional confirmation comes from Fig. 7. The chaotic wave field here is calculated for $k = 0.25$. The group velocity in this case is $v_{gr} \approx -2.65$. The filaments and the orientation of the maxima in numerical simulations have the direction predicted by this value, although quantitatively deviations from the predictions of Eq. (7) can be larger than in the cases $k = 2$ and $k = 0.8$. Some of the elongated structures of double maxima have roughly the same profile as the rogue wave shown in Fig. 4, as the one encircled by a black ellipse in the figure.

V. COUNTING BIG WAVES

In order to find the waves with highest amplitudes in the chaotic wave fields shown above we used the following procedure. In each numerical run, we took the function $|\psi(x)|$ at each fixed τ and found the absolute maximum of it as a function of x. The typical numerical x interval in these simulations was chosen close to $[-100,100]$. Plotting these maxima as a function of τ allowed us to find the largest waves in the whole run. One subtlety in these simulations is that the initial plane wave should be kept periodic on the numerical grid. In order to satisfy this condition, the total grid length must contain an integer number of periods. In other words, the numerical grid should have a length of $(2N\pi/k)$, with N being a sufficiently large positive integer.

One of these functions for $k = 0.8$ is shown in Fig. 8 by the blue dashed curve. The curve starts at the background level $|\psi| = 1$. The initial exponential growth of the curve is caused by the modulation instability. The curve reveals several maxima that are 2.5–3 times higher than the amplitude of the original plane wave. These maxima can be attributed to rogue waves in this chaotic wave field. For the sake of comparison, we also provide the curve that corresponds to

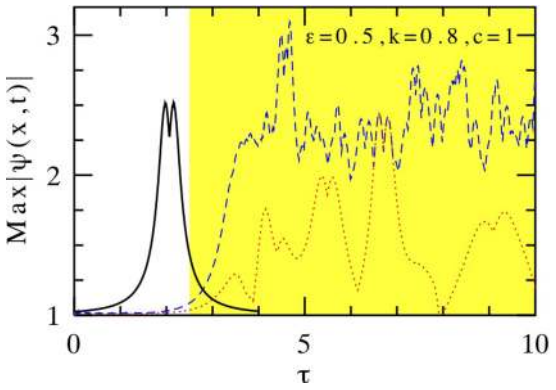

FIG. 8. (Color online) Absolute maximum of the chaotic wave-field amplitude in x as a function of τ in the case $k = 0.8$. The blue dashed (upper) and red dotted (lower) curves are obtained using either the whole numerical x interval or a smaller portion of it. The black solid curve on the left is the exact rogue-wave solution ($x = const$) given in Fig. 3. The yellow part (in the interval $2.5 < \tau < 10$) is the region of chaotic waves beyond modulation instability. It is the same region as shown along the vertical axis in Fig. 6.

the exact SSE rogue-wave solution presented in Fig. 3. It is shown in Fig. 8 by the black two-peaked curve. As we can see, the amplitudes of rogue waves generated by the chaotic wave field are comparable or exceed the amplitude of the exact rogue-wave solution. The strongest rogue wave in this plot appears at τ value slightly below $\tau = 5$. Its exact position on the x axis can be found investigating the function $|\psi(x)|$ for this value of τ.

The blue dotted line in Fig. 8 is constructed using the data obtained with the numerical grid along the x axis equal to 157 in the dimensionless units. Clearly, when selecting narrower intervals along the x axis in calculations, some maxima are missed. Thus, the whole curve can then be lower than the blue line. An example of such reduction is the red dotted curve in Fig. 8. It is located well below the blue curve except some of the maxima that remain in the narrower interval. Even in this case, the remaining rogue-wave amplitude is comparable with the amplitude of the exact solution, which is around the level of 2.5. It is also worthy to mention that some maxima in this figure appear in pairs although not necessarily strictly symmetric. When this happens, the maxima belong to one of the rogue-wave structures in the form of double red spots well visible in Fig. 6. This is also consistent with the double-peak profile of the exact solution for rogue waves shown in Fig. 3.

VI. PROBABILITY DENSITY FUNCTIONS

The probability of having a wave of certain peak amplitude (A) in the chaotic wave field provides us with important information about the field itself and the rogue waves in particular. We constructed these probabilities based on the total wave field using as many numerical data as possible. Namely, we counted all local maxima of the chaotic wave fields generated as described above. Naturally, figures in the previous sections showed only a small part of the numerical results. Comparison of the blue and red curves in Fig. 8 shows that having large data sets is essential. The probability density functions (PDFs) presented below are based on significantly larger data sets than shown above.

In plotting the PDFs, there are different approaches used for surface water waves and in optics. In each case, the envelope function that satisfies the evolution equation contains a faster oscillating wave with certain carrier frequency. When we are dealing with water waves, the value of interest is the crest to trough height of the wave, which is roughly equal to twice the envelope amplitude. In the case of optical waves, the measurable quantity is the optical intensity, which is given by the amplitude square of the envelope. Thus, PDFs in each of these cases can be constructed either plotting the wave height, which is twice the amplitude or intensity, which is the squared amplitude. As we do not apply our results to any of these cases, we provide here more general PDFs plotting along the horizontal axis the amplitude, which is the modulus of the complex envelope. These curves can be recalculated into more practically oriented PDFs keeping in mind these simple rules.

For each value of k under consideration, we used several thousands of independent realizations. In order to increase the number of maxima we considered the field at a discrete number of values of τ for each realization and found all local maxima of the field amplitude varying just x. In all these cases we discarded the initial MI stages of evolution. Besides, we did not count small-amplitude waves and discarded all maxima with amplitude below 0.1. The amplitude of the initial plane wave is one and all amplitudes are relative to this reference. Typically, for each plot, the data we dealt with consisted of several tens of millions of maxima, which allowed us to obtain relatively smooth statistical curves. The exception is the high-amplitude parts of the curves, where data become scarce due to its low probability.

An example of PDF constructed this way is shown in Fig. 9. Here, we used $k = 2$. The red curve shows the probability, in logarithmic scale, of having a wave with a given peak amplitude in the chaotic wave field. The low-amplitude part of the curve is neglected as explained above. The high-amplitude part of the curve still has a random component due to the insufficient data. However, by averaging this part we can estimate that it can be approximated by a smooth exponentially decaying tail. The amplitude of the exact rogue-wave solution for the same value of k is shown in the plot by the vertical

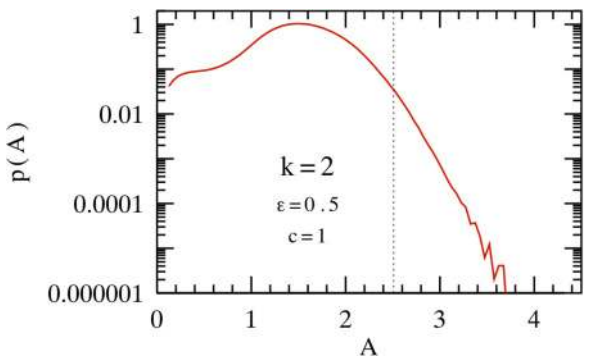

FIG. 9. (Color online) Probability density function for the case $k = 2$. The peak amplitude of the analytic rogue-wave solution presented in Fig. 2 is marked here by the dotted vertical line.

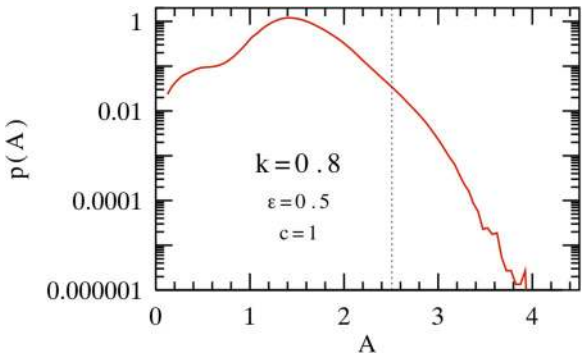

FIG. 10. (Color online) Probability density function for the case $k = 0.8$. The peak amplitude of the rogue-wave solution presented in Fig. 3 is shown by the dotted vertical line.

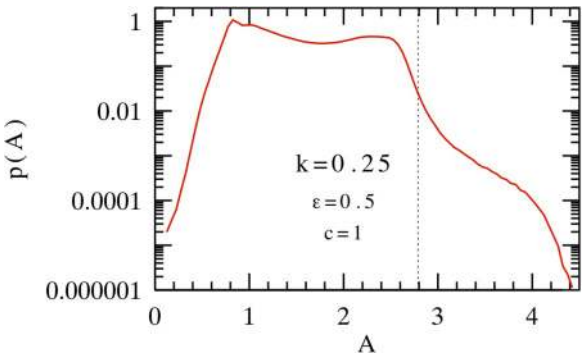

FIG. 11. (Color online) Probability density function for the case $k = 0.25$. The peak amplitude of the rogue-wave solution presented in Fig. 4 is shown by the dotted vertical line.

dotted line. As we can see, a significant number of the field maxima lies above this line.

Similar PDF curve is obtained for the case $k = 0.8$. It is shown in Fig. 10. Qualitatively, it has a shape very similar to the one for $k = 2$. A noticeable difference is the slightly elevated number of events above the theoretical rogue-wave amplitude shown by the vertical dotted line. In addition, the curve extends up to the amplitude $A \approx 4$, while in the previous case the upper limit for the maximal observed amplitude is slightly lower.

Significant differences appear at lower values of k. The PDF for $k = 0.25$ is shown in Fig. 11. The shape of this PDF cannot be described by any known statistical functions. Instead of a single maximum probability for a certain peak amplitude, it has an almost flat top in the interval [0.8,2.6], below the rogue-wave threshold. Despite the fact that the corresponding rogue-wave amplitude (2.8) is now higher than in the two previous cases ($\approx$2.5), a significant number of waves have even higher amplitudes. The whole tail of this PDF is elevated and the maximal presented peak-amplitude goes up to 4.4 while in the previous cases this value was below 4. For the sake of comparison we used the same horizontal and vertical scales in all three figures.

All PDFs can be approximated by an exponential tail that does not prevent appearance of waves with even higher amplitudes than in the three plots shown above. Indeed, in one of our simulations with $k = 0.25$, we observed the highest amplitude, which was slightly higher than 5, i.e., well beyond the scale of Fig. 11. Clearly, the high-amplitude parts of these curves can be continued further but need special techniques to be accurate.

Although our study is far from being complete, it shows clearly that higher-order terms in the evolution equation have a significant influence on both the shape of the big waves and the probability of their appearance. We have chosen the coefficient ϵ in the Sasa-Satsuma equation to be not very small (0.5) in order for these differences to be more noticeable. This equation is convenient for analytic studies as it keeps the integrability for an arbitrary value of ϵ. However, we expect that higher-order terms in proportions different from the SSE case may also have significant influence on the probabilities of big-wave appearance. Further steps in these studies with specific cases of practical interest should be done in future.

VII. CONCLUSIONS

To conclude, we studied the properties of the chaotic wave fields generated by the Sasa-Satsuma equation. We have found that the filaments of the self-focused fields generated due to modulation instability propagate in the direction roughly defined by the group velocity calculated from the dispersion relation for the plane-wave solution. These results provide an explanation for the skewed shape of the rogue waves given by the exact solutions.

The calculation of the probability density functions for various values of the initial wavenumber shows that smaller values of k result in elevated probability of high-amplitude waves. Our results demonstrate the importance of the higher-order terms in the evolution equation that may lead to higher probabilities of rogue waves in a chaotic wave field.

ACKNOWLEDGMENTS

The authors acknowledge the support from the Volkswagen Stiftung. N.D. and N.A. acknowledge the support of the Australian Research Council (Discovery Project DP140100265). N.A. acknowledges support through the Alexander von Humboldt Award (Germany). The work of J.M.S.C. is supported by the MINECO, under Contracts No. FIS2009- 09895 and No. TEC2012-37958-C02-02.

[1] M. Onorato, S. Residori, U. Bortolozzo, A. Montina, and F. T. Arecchi, Phys. Rep. **528**, 47 (2013).

[2] M. Onorato, D. Proment, G. Clauss, and M. Klein, PLOS ONE **8**, e54629 (2013).

[3] N. Akhmediev and E. Pelinovsky (eds.), Eur. Phys. J., Special Topics **185**, 266 (2010).

[4] N. Akhmediev, J. M. Dudley, D. R. Solli, and S. K. Turitsyn, J. Optics **15**, 060201 (2013).

[5] P. Müller, Ch. Garrett, and A. Osborne, Oceanography **18**, 66 (2005).
[6] K. Dysthe, H. E. Krogstad, and P. Müller, Annu. Rev. Fluid Mech. **40**, 287 (2008).
[7] N. Akhmediev, A. Ankiewicz, J. M. Soto-Crespob, and J. M. Dudley, Phys. Lett. **375**, 541 (2011).
[8] C. Kharif and E. Pelinovsky, Eur. J. Mech. B/Fluids **22**, 603 (2003).
[9] A. R. Osborne, M. Onorato, and M. Serio, Phys. Lett. A **275**, 386 (2000).
[10] C. Garrett and J. R. Gemmrich, Phys. Today **62**, 62 (2009).
[11] Y. Ohta and J. Yang, Proc. R. Soc. A **468**, 1716 (2012).
[12] A. Calini and C. M. Schober, J. Opt. **15**, 105201 (2013).
[13] P. Dubard, P. Gaillard, C. Klein, and V. B. Matveev, Eur. Phys. J. Spec. Top. **185**, 247 (2010).
[14] P. Dubard and V. B. Matveev, Nat. Hazards Earth Syst. Sci. **11**, 667 (2011).
[15] L. Stenflo and M. Marklund, J. Plasma Phys. **76**, 293 (2010).
[16] D. R. Solli, C. Ropers, P. Koonath, and B. Jalali, Nature **450**, 1054 (2007).
[17] A. Montina, U. Bortolozzo, S. Residori, and F. T. Arecchi, Phys. Rev. Lett. **103**, 173901 (2009).
[18] K. Hammani, B. Kibler, C. Finot, and A. Picozzi, Phys. Lett. A **374**, 3585 (2010).
[19] W. M. Moslem, P. K. Shukla, and B. Eliasson, Europhys. Lett. **96**, 25002 (2011).
[20] Zh. Yan, Commun. Theor. Phys. **54**, 947 (2010).
[21] N. Akhmediev, A. Ankiewicz, and M. Taki. Phys. Lett. A **373**, 675 (2009).
[22] D. J. Kedziora, A. Ankiewicz, and N. Akhmediev, Phys. Rev. E **84**, 056611 (2011).
[23] D. J. Kedziora, A. Ankiewicz, and N. Akhmediev, Phys. Rev. E **88**, 013207 (2013).
[24] D. J. Benney and A. C. Newell, J. Math. Phys. **46**, 133 (1967).
[25] V. E. Zakharov, J. Appl. Mech. Tech. Phys. **9**, 190 (1968).
[26] A. Ankiewicz, Yan Wang, S. Wabnitz, and N. Akhmediev, Phys. Rev. E **89**, 012907 (2014).
[27] Yu. V. Sedletskii, J. Exp. Theor. Phys. **97**, 180 (2003).
[28] A. V. Slunyaev, J. Exp. Theor. Phys. **101**, 926 (2005).
[29] M. J. Potasek and M. Tabor, Phys. Lett. A **154**, 449 (1991).
[30] S. B. Cavalcanti, J. C. Cressoni, H. R. da Cruz, and A. S. Gouveia-Neto, Phys. Rev. A **43**, 6162 (1991).
[31] M. Trippenbach and Y. B. Band, Phys. Rev. A **57**, 4791 (1998).
[32] N. Sasa and J. Satsuma, J. Phys. Soc. Japan **60**, 409 (1991).
[33] D. Mihalache, L. Torner, F. Moldoveanu, N.-C. Panoiu, and N. Truta, J. Phys. A: Math. Gen. **26**, L757 (1993).
[34] D. Mihalache, N.-C. Panoiu, F. Moldoveanu, and D.-M. Baboiu, J. Phys. A: Math. Gen. **27**, 6177 (1994).
[35] D. Mihalache, L. Torner, F. Moldoveanu, N.-C. Panoiu, and N. Truta, Phys. Rev. E **48**, 4699 (1993).
[36] O. C. Wright III, Chaos, Solitons Fractals **33**, 374 (2007).
[37] A. Sergyeyev and D. Demskoi, J. Math. Phys. **48**, 042702 (2007).
[38] C. Gilson, J. Hientarinta, J. Nimmo, and Y. Ohta. Phys. Rev. E **68**, 016614 (2003).
[39] J. Kim, Q-H. Park, and H. J. Shin, Phys. Rev. E **58**, 6746 (1998).
[40] U. Bandelow and N. Akhmediev, Phys. Lett. A **376**, 1558 (2012).
[41] Shihua Chen, Phys. Rev. E **88**, 023202 (2013).